

Characteristic evaluation on spray-deposited WFTO thin films as a function of W doping ratio

G. Turgut*, E. F. Keskenler, S. Aydın,
D. Tatar, E. Sonmez, S. Dogan, B. Duzgun

Received: 14 December 2012/Revised: 27 March 2013/Accepted: 2 April 2013/Published online: 16 May 2013
© The Nonferrous Metals Society of China and Springer-Verlag Berlin Heidelberg 2013

Abstract In this work, F and F + W simultaneously doped SnO₂ highly transparent conducting thin films were deposited on glass substrates at (500 ± 5) °C temperature by the spray pyrolysis method. Microstructural, morphological, electrical and optical properties of FTO films were investigated as a function of tungsten (W) doping, in the range from 0 to 5 at%. X-ray diffraction patterns show that the films exhibit a tetragonal cassiterite structure and (200) preferential orientation of FTO film, and the relative strength of these peaks changes with altering the W doping ratio. The preferred growth of (211) changed to (200) plane with 2 at% W doping level and 3 at% W-doped film had (200) orientation and with further doping, this changed to (110) orientation. The scanning electron microscopy and atomic force microscopy images of the films indicate that the films are made up of dense small particles of a pyramidal shape and have a smooth surface. It was observed that the surface morphology of the films did not change much when the W element was inserted to the FTO structure. It was found that the sheet resistance values of the films varied with W doping ratio, and 2 at% W-doped FTO thin film exhibited the lowest values of sheet resistance (1.12 Ω). Also, the highest figure of merit, infrared reflectivity and optical band gap values were

calculated for 2 at% W-doped FTO film as $50.9 \times 10^{-2} \Omega^{-1}$, 98.82 % and 4.13 eV, respectively. These results make the films an effective candidate for usage in many optoelectronic applications and photo-thermal conversion of solar energy.

Keywords WFTO; FTO; Spray pyrolysis; Thin films; Lattices

1 Introduction

Transparent conductive oxides such as SnO₂, In₂O₃, ZnO and TiO₂ have been widely used in optic and electronic devices [1, 2]. In the last few decades, there has been a rising interest in the use of transparent conducting oxide thin films in the field of conducting solar window materials as thin film solar cells [3], heat reflectors in solar applications [4, 5], gas sensors [6, 7], energy storage for batteries and photo-electrodes of dye-sensitized solar cells [8, 9]. Their low electrical resistivity, high transmittance in the visible range and infrared (IR) reflectivity, chemical inertness, mechanically hard property [10, 11] and adherence to the many substrates are several advantages. Amongst them, tin oxide (TO, SnO₂) is the one of first transparent conductors to achieve significant commercialization [10, 12]. Although the stoichiometric TO is a good insulator, the non-stoichiometric TO is an n-type semiconductor because of intrinsic defects such as oxygen vacancies or tin interstitials [13–16]. In order to control and improve the properties of SnO₂, many studies have been conducted on doping SnO₂. The doping of the SnO₂ could be carried out by changing Sn⁴⁺ and O²⁻ atoms with dopant atoms. The efficiency of dopant atoms depends on the difference between the ionic radius of the host and the dopant atoms [16]. Both tungsten (W) and fluorine (F) come amongst the most important elements of anion and cation

G. Turgut*, S. Aydın, D. Tatar, E. Sonmez, B. Duzgun
Department of Physics Education, Kazim Karabekir Education
Faculty, Atatürk University, Erzurum 25240, Turkey
e-mail: guventurgut@atauni.edu.tr

E. F. Keskenler
Department of Nanotechnology, Faculty of Engineering,
Recep Tayyip Erdoğan University, Rize 53100, Turkey

S. Dogan
Department of Electrical and Electronics Engineering,
Faculty of Engineering and Architecture, Balikesir University,
Balikesir 10145, Turkey

dopants. Tungsten has W^{6+} state and the radius of W^{6+} is proper to that of Sn^{4+} (W^{6+} : 67 pm; Sn^{4+} : 71 pm); with this property, it is easy to replace the Sn^{4+} theoretically [17, 18]. Similarly, the ionic radii of fluorine (F) is similar to that of oxygen (F^- : 131 pm; O^{2-} : 138 pm) [19] and F atoms easily indwells in the place of oxygen [20]. In case W^{6+} and F^- are changed by Sn^{4+} and O^{2-} , respectively, in SnO_2 crystal structures, W and F atoms will give two and one extra free electrons to SnO_2 structure, respectively. Thus, both atoms of fluorine and tungsten give three free electrons to SnO_2 lattice [21, 22] and can increase the visible transmittance, IR reflectance and electrical conductivity.

SnO_2 thin films can be deposited by several techniques such as thermal evaporation [12], sputtering [23], chemical vapour deposition [24], spray pyrolysis [22], the hydrothermal method [25], pulsed plasma deposition (PPD) [26], pulsed laser deposition [27], reactive evaporation [28] and the sol-gel spin coating technique [18]. Amongst these deposition techniques, spray pyrolysis is a useful method to fabricate thin films because of its simple and cheap experimental arrangement [29], easy adding of doping elements, reproducibility, high growth rate and mass production capability [30]. In this study, we intended to investigate the effect of W doping on the structural, morphological, optical and electrical properties of $SnO_2:F$ films on glass substrates at (500 ± 5) °C temperature deposited via spray pyrolysis.

2 Experimental

2.1 Synthesis

F and W/F doubly doped TO thin films, given in the present study, were fabricated using a homemade spray pyrolysis apparatus. $0.7 \text{ mol}\cdot\text{L}^{-1}$ stannous chloride dehydrate ($SnCl_2\cdot 2H_2O$) dissolved in ethyl alcohol (C_2H_5OH) was prepared as the SnO_2 starting material and a few drops of HCl were added to this. For F and W doping, ammonium fluoride (NH_4F) dissolved in deionized water and tungsten hexachloride (WCl_6) dissolved in ethyl alcohol were used as the dopant materials. These materials were used in necessary amounts to prepare 20 at% F-doped and 20 at% F + 1 at%–5 at% (varied with 1 at% step) W-doped SnO_2 samples and six different spray solutions were prepared. All the spray solutions were magnetically stirred for 2 h to obtain homogenous solutions. The resultant solutions were sprayed on glass substrates at (500 ± 5) °C temperature. The glass substrates were firstly kept in boiling chromic acid solution and then they were rinsed with deionized water. Finally, they were cleaned with acetone, deionized water and methanol using an ultrasonic cleaner and dried with nitrogen. The normalized distance between the spray nozzle and the substrates

(40 cm), the flow rate ($10 \text{ ml}\cdot\text{min}^{-1}$) and every total spray solutions' quantity (30 ml) were kept fixed. Filtered compressed air was used as carrier gas. The total deposition time was maintained at 3 min for each film. The substrate temperature (working temperature) was (500 ± 5) °C. The substrate temperature was maintained using a k-type thermocouple based on a digital temperature controller. After deposition, the coated substrates were allowed to cool down naturally to room temperature. In each process, five more samples were produced simultaneously at each doping level. The sprayed samples were named as 20 at% F-doped FTO, 20 at% F + 1 at%–5 at% W-doped WFTO-1, -2, -3, -4 and -5.

2.2 Characterizations

The structural characterization of the SnO_2 thin films was carried out by X-ray diffraction (XRD) measurements using a Rigaku Miniflex II diffractometer with $Cu \text{ K}\alpha$ radiation ($\lambda = 0.15418 \text{ nm}$). The diffractometer reflections were taken at room temperature and the values of 2θ were altered between 10° and 90° . The morphological properties of the samples were determined by means of a Zeiss Evo LS10 scanning electron microscope (SEM) and an atomic force microscope (AFM, which was produced by Nanomagnetics Instrument). The sheet resistance values were measured by a four-point probe. The optical transmittance measurements of the samples was recorded in the spectral region of 290–1,100 nm at 300 K using a UV–VIS spectrometer (Perkin-Elmer, Lambda 40) which works in the range of 200–1,100 nm.

3 Results and discussions

3.1 Microstructural properties

The structural properties of FTO and WFTO thin films have been studied using XRD spectra. Typical XRD spectra of the films are showed in Fig. 1. All diffractograms show only characteristic SnO_2 peaks with cassiterite tetragonal structure and these peaks collaborate with the ones from JCPDS card No.: 1-1445. Other peaks belonging to SnF_2 , SnO , Sn_2O_3 and metallic W are not observed in the samples. The calculated d' values of FTO and WFTOs films are given in Table 1, and these values are compared with the standard ones from the JCPDS card No.: 41-1445. It is perceptible from the figure that the FTO films grow along the preferred orientation of (200), whereas 1 at% W-doped FTO films grow along (211). The preferred growth is (200) plane with 2 at% W doping content. The films doped with 3 at% W have (200) orientation and a

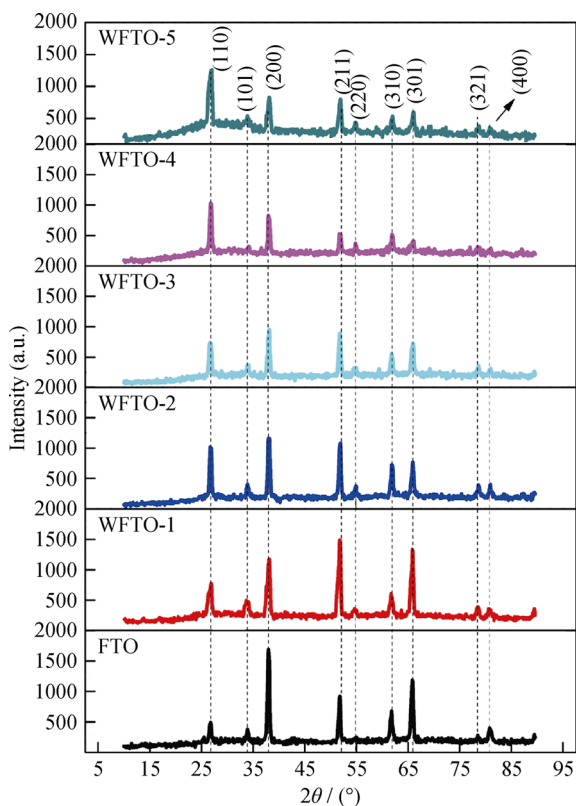


Fig. 1 XRD patterns of FTO and WFTOs thin films

further doping ratio has (110) orientation. The other observed peaks are (101), (220), (310), (301), (321) and (400). It can be seen from Fig. 1 that the intensities of all peaks decrease with increasing W doping content. The (101), (211) and (301) preferential orientations have been observed by Gordillo et al. [31]. A relationship between the precursor solution chemistry and the preferential direction for the growing of SnO₂ films was found. In another study, Smith et al. [32] analysed the relation between solution chemistry and film morphology by preparing SnO₂ films with and without the addition of HCl in SnCl₂·2H₂O solution. It was concluded that when HCl was added with the starting solution, the films were highly oriented along (200) plane. Agashe et al. [33] reported a change in the preferred orientation from (110) to (200) as the concentration of tin chloride increased in the precursor solution, and they concluded that the change of preferential orientation was caused by the gradual incorporation of Sn at interstitial sites in the SnO₂ lattice. Elangovan and Ramamurthi [34] found that (211) preferential orientation of pure SnO₂ changed to (200) orientation with F doping. In another study reported by Elangovan and Ramamurthi [35], (211) preferential orientation of undoped films changed to (200) line with F doping and for Sb doping films, (211) line firstly changed to (301) plane at low doping content (1.0 and 1.5 wt% Sb content) and then

changed to (200) line at high Sb doping content. They also reported that preferential orientation depended on precursor solution content. A change at the preferential orientation was found as a function of the spray precursor solution molarity by Babar et al. [36]. They found that when the solution molarity of Sb-doped SnO₂ was changed from 0.5 to 2.5 mol·L⁻¹, the preferential orientation changed from (110) to (200), (301) and (211) planes. From the studies of un- and doped SnO₂ films by Chacko et al. [37] and Lin et al. [38], it was found that the substrate temperature on the spray pyrolysis was a factor in affecting the preferential orientation. Thus, we can conclude the following: during the thin film deposition, the grains of TO were oriented to have minimum interfacial energy [39]. At the film deposition by spray pyrolysis, the growth direction depends on the properties of the material under study and its deposition conditions such as substrate temperature, doping materials, its content and film thickness. In this study, the change of preferential orientation can be sought in the differences of the preparation of the starting solutions with W doping ratio. Similar to our results for preferential orientation, in the literature, F-doped SnO₂ films grew along (200) orientation obtained by Agashe and Major [40]. Undoped and F-doped films grown along the (110) orientation were found by Patil et al. [41] and Zaouk et al. [42], respectively. Shanthi et al. [43] observed that the preferred orientation remains along (110) for all conditions, irrespective of the substrate temperature, film thickness, solution flow rate, air flow rate, substrate to nozzle distance and fluorine doping level. The (211) and (110) lines were observed by Babar et al. [44] and Yao [45] for Sb-doped SnO₂ films. Also, Huang et al. [21] found (110) preferential orientation for W-doped SnO₂ films prepared by PPD.

The lattice constants *a* and *c* of the tetragonal phase are determined using following relation [37]:

$$\frac{1}{d^2} = \left(\frac{h^2 + k^2}{a^2} \right) + \left(\frac{l^2}{c^2} \right) \tag{1}$$

where *d* is the interplanar distance and *h*, *k* and *l* are Miller indices. The calculated lattice constants can be seen in Table 2. The calculated *a* and *c* values nearly agree with the ones from JCPDS card No.: 41-1445 (*a* = *b* = 0.47382 nm, *c* = 0.31871 nm). It is seen from the Table 2 that the lattice parameters are not affected much by the incorporation of the W dopants in the films.

The average grain size is calculated for the most striking peaks using Scherrer formula [46]:

$$D = \frac{0.9\lambda}{\beta \cos \theta} \tag{2}$$

where *D* is the grain size of nanoparticles, *β* is the full width at half of the peak maximum in radians and *θ* is the

Table 1 The interplanar distance (d) values of FTO and WFTO thin films (nm)

| hkl | Standard | FTO | WFTO-1 | WFTO-2 | WFTO-3 | WFTO-4 | WFTO-5 |
|-------|----------|---------|---------|---------|---------|---------|---------|
| 110 | 0.33470 | 0.33435 | 0.33504 | 0.33428 | 0.33474 | 0.33358 | 0.33441 |
| 101 | 0.26427 | 0.26492 | 0.26570 | 0.26465 | 0.26446 | 0.26371 | 0.26521 |
| 200 | 0.23690 | 0.23728 | 0.23725 | 0.23677 | 0.23693 | 0.23698 | 0.23689 |
| 211 | 0.17641 | 0.17681 | 0.27695 | 0.17657 | 0.17672 | 0.17665 | 0.17655 |
| 220 | 0.16750 | 0.16767 | 0.16803 | 0.16750 | 0.16764 | 0.16757 | 0.16781 |
| 310 | 0.14984 | 0.15026 | 0.15037 | 0.15006 | 0.15018 | 0.15000 | 0.14987 |
| 301 | 0.14155 | 0.14202 | 0.14203 | 0.14184 | 0.14184 | 0.14176 | 0.14172 |
| 321 | 0.12147 | 0.12189 | 0.12189 | 0.12176 | 0.12175 | 0.12184 | 0.12172 |
| 400 | 0.11844 | 0.11891 | 0.11895 | 0.11883 | 0.11830 | 0.11897 | 0.11882 |

Table 2 The structural and element composition properties of FTO and WFTO thin films

| Samples | Lattice constants/nm | | Grain size, D /nm | Dislocation density [$\delta/(10^{15} \text{ lines}\cdot\text{m}^{-2})$] | F/Sn ratio/at% | W/Sn ratio/at% |
|---------|----------------------|---------|---------------------|--|----------------|----------------|
| | a | c | | | | |
| FTO | 0.47420 | 0.32191 | 19.15 | 2.73 | 22.34 | – |
| WFTO-1 | 0.47477 | 0.32124 | 19.55 | 2.62 | 24.96 | 1.26 |
| WFTO-2 | 0.47364 | 0.32153 | 17.26 | 3.36 | 18.15 | 2.78 |
| WFTO-3 | 0.47408 | 0.32066 | 18.76 | 2.84 | 25.72 | 3.83 |
| WFTO-4 | 0.47350 | 0.32170 | 25.08 | 1.59 | 24.71 | 4.42 |
| WFTO-5 | 0.47382 | 0.32082 | 18.62 | 2.89 | 25.20 | 5.58 |

Bragg's angle. The grain size values are given in Table 2 and these values do not change much with W doping.

The stress is one of the most important factors negatively affecting the structural properties, which may be a result of geometric mismatch at interphase boundaries between the crystalline lattices of films and the substrate [47]. The stresses can cause crystal disorders and dislocations in the films. And, the dislocation density (δ) can be defined as the length of dislocation lines per unit volume ($\text{lines}\cdot\text{m}^{-2}$). The dislocation density (δ) of the films is calculated using the following relation [48]:

$$\delta = 1/D^2 \quad (3)$$

The calculated dislocation density values are given in Table 2. The calculated δ value of $2.73 \times 10^{15} \text{ lines}\cdot\text{m}^{-2}$ for FTO film slightly decreases to $2.62 \times 10^{15} \text{ lines}\cdot\text{m}^{-2}$ then increases to $3.36 \times 10^{15} \text{ lines}\cdot\text{m}^{-2}$ and again decreases to 2.84×10^{15} , $1.59 \times 10^{15} \text{ lines}\cdot\text{m}^{-2}$ for 1 at%, 2 at%, 3 at% and 4 at% W doping ratios. And, the final value is $2.89 \times 10^{15} \text{ lines}\cdot\text{m}^{-2}$ for 5 at% W-doped FTO sample.

3.2 Morphological and surface composition properties

The surface morphology and element compositions of F and F + W doubly doped SnO_2 films are investigated by SEM micrographs and EDX spectra shown in Fig. 2a–f. These spectra clearly confirm the existence of Sn, O, F and W elements on the surface of FTO and WFTO films. EDX

analysis shows that the atomic ratios of F/Sn (at%) in spray-deposited FTO, WFTO-1, -2, -3, -4, -5 films are found to be 22.34, 24.96, 18.95, 25.72, 24.71, 25.20, respectively. These values are slightly more than the ones used in the spray solution. For WFTO samples, W doping ratios (W/Sn [at%]) are found to be 1.26, 2.78, 3.83, 4.42 and 5.58. As seen from Fig. 2, FTO and WFTO films are composed of dense small particles of a pyramidal shape and have a smooth surface. Also, the FTO film has well-formed and densely packed crystallites and the distribution of these particles is homogenous. It is observed that surface morphology of the films does not change much when W element is inserted into the FTO structure. The grain size of FTO film slightly increases with 1 at% W doping and for 2 at% W-doped film, a few big grains appear on the smaller particles. Increasing to 3 at% W content, the film morphology becomes homogenous and the size of small grains increases. The morphology of 4 at% W-doped FTO film is non-homogenous. The surface of films becomes smooth and homogenous with 5 at% W content. This particles structure is similar to those obtained in other studies [49–52].

The surface morphology of the films has also been examined by AFM. AFM images are obtained at $5 \mu\text{m} \times 5 \mu\text{m}$ planar in tapping mode, at 512×512 resolutions and with $1 \mu\text{m}\cdot\text{s}^{-1}$ of scanning speed. 2- and 3D AFM images of the films with different tungsten doping concentrations are shown in Fig. 3a–f. From the AFM

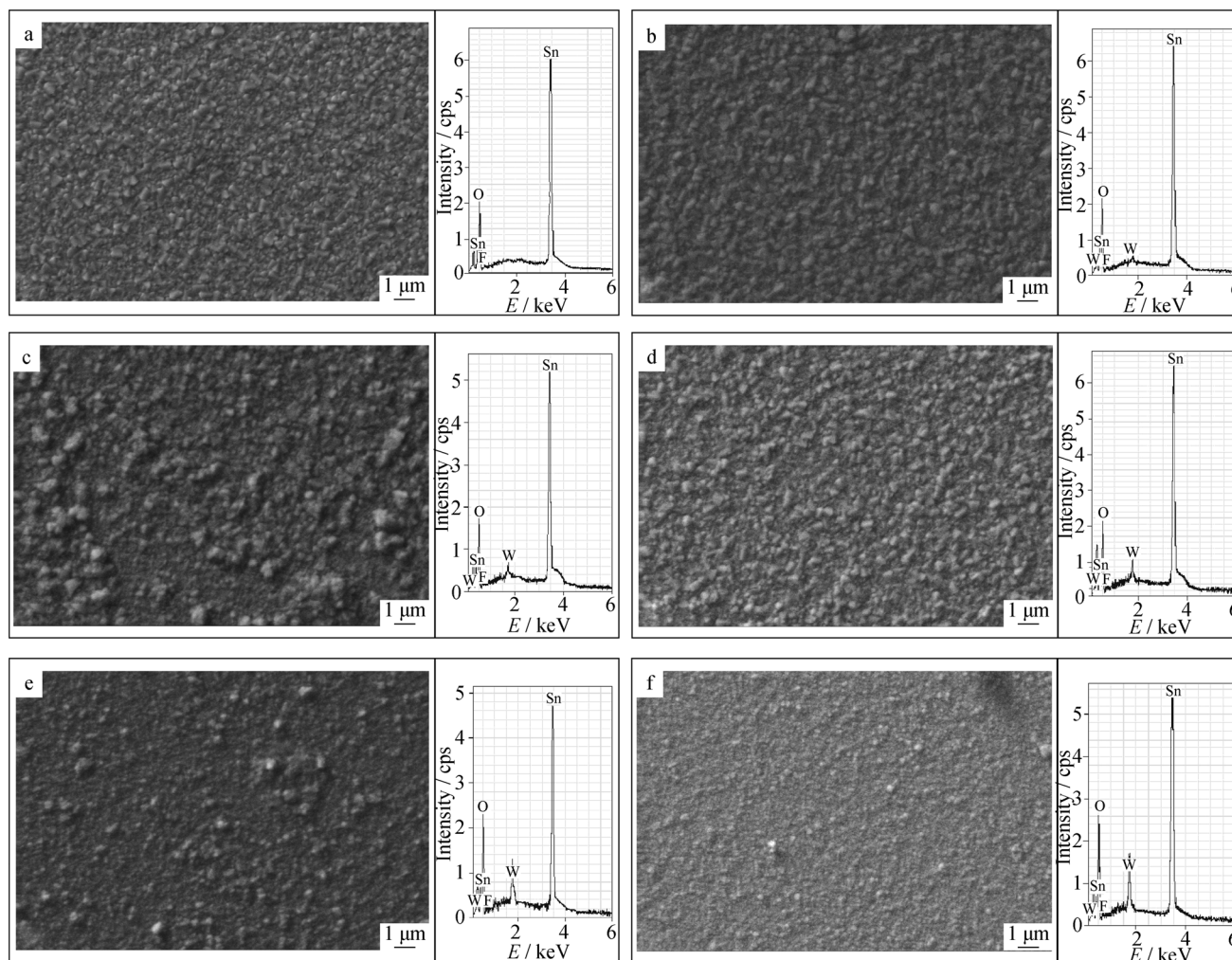


Fig. 2 SEM images and EDX spectra of FTO and WFTOs thin films: **a** FTO, **b** WFTO-1, **c** WFTO-2, **d** WFTO-3, **e** WFTO-4 and **f** WFTO-5

images, the films are composed of nanoparticles which almost homogeneously distribute on the film surfaces. It can also be observed that the surface morphology of the films does not change much when W element is inserted into the FTO structure. Root mean square (*RMS*) roughness values of the films have been extracted from the AFM data. The *RMS* values of FTO films are found to be 106 nm and this value decrease to 73.1 and 64.7 nm for 1 at% and 2 at% W-doped films, respectively. As the doping levels increased from 2 at% to 5 at%, the roughness of the films continuously increased from 64.7 to 138 nm. A detailed AFM study reveals that the roughness of the film is dependent on the dopant level and the smoothest surface is obtained for 2 at% W-doped FTO film.

3.3 Electrical properties

It is found that the all samples have an n-type conduction mechanism using the hot probe method. The electrical properties of FTO and WFTOs films have been identified

by the four-point probe method. The sheet resistance values of the films are given in Table 3 and in Fig. 4. As seen in Fig. 4, there is a decrease in the sheet resistance and resistivity of FTO film with W doping up to 2 at%. The sheet resistance values of FTO films decrease from 3.22 to 2.33 and 1.12 Ω for 1 at% and 2 at% W doping ratio, respectively. When the doping ratio is increased further, the sheet resistance values continuously increase and reach maximum values of 4.53 Ω for 5 at% W-doped FTO. The variation in the sheet resistance of F-doped TO thin films with tungsten doping can be explained by the presence of a different valence state of W element. When $\text{SnO}_2:\text{F}$ films are doped with W at low doping content, some of the Sn^{4+} in the lattice is replaced by W^{6+} due to the ionic radius of Sn^{4+} being similar to the radius of W^{6+} (W^{6+} : 67 pm; Sn^{4+} : 71 pm) [53], resulting in a decrease in the sheet resistance [17, 18, 21, 26]. Hence, a reduction in the sheet resistance is observed until the W concentration reaches 2 at%. Beyond 2 at% of W doping, some of the W^{6+} is reduced to the low valence states, in which the ionic radius

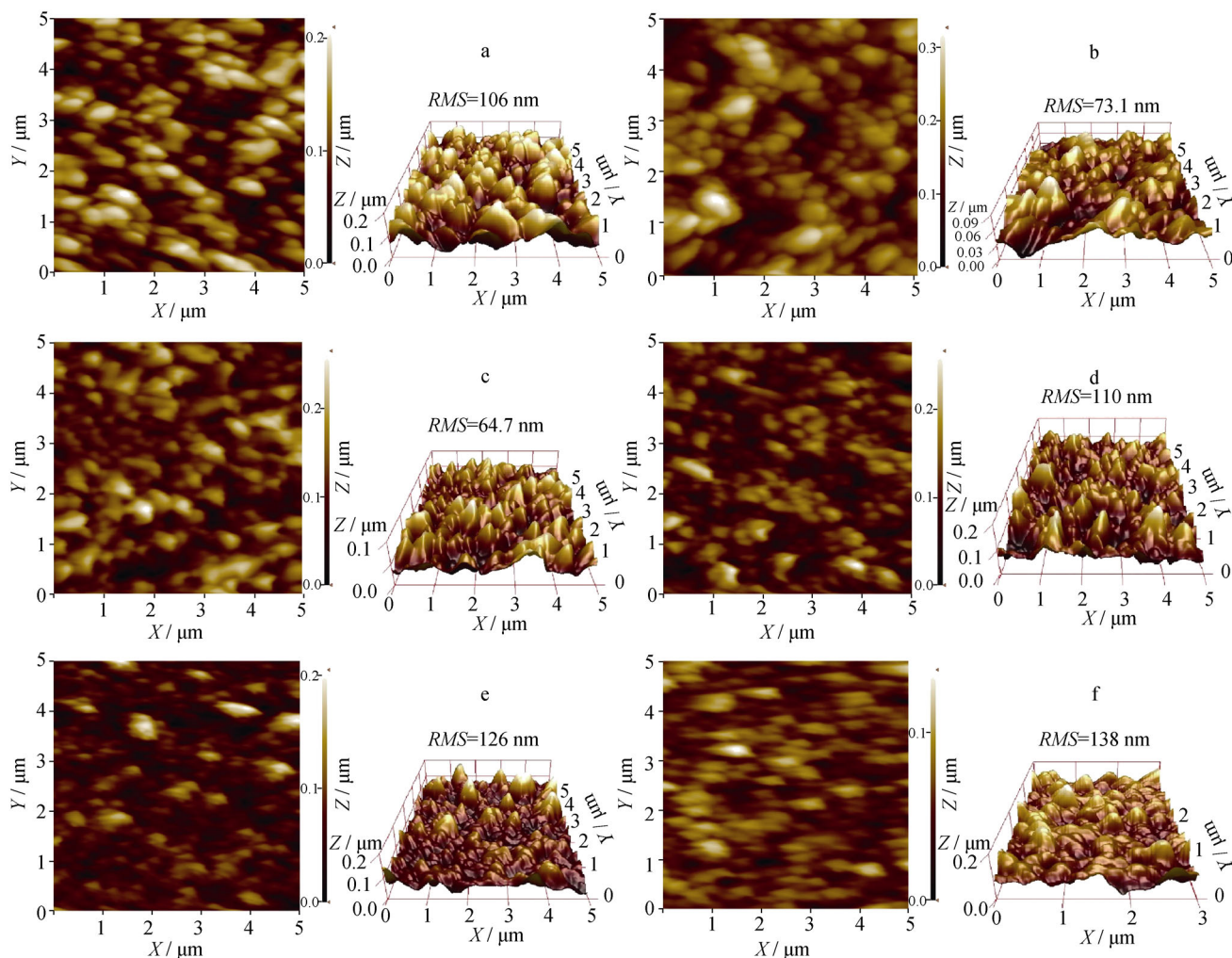


Fig. 3 2- and 3D AFM images of FTO and WFTOs thin films: **a** FTO, **b** WFTO-1, **c** WFTO-2, **d** WFTO-3, **e** WFTO-4 and **f** WFTO-5

is more than that of Sn^{4+} [53–55], resulting in the formation of acceptor states and a loss of carriers and thus, in present study, an increasing in sheet resistance. Another reason for increasing sheet resistance may be shown as both F and W dopants may not be placed in the proper lattice position with increasing W doping. In earlier studies, it has been found that 3 at% and 3 wt% W doping reduced the sheet resistance of SnO_2 and tungsten atoms are fully oxidized to the valence of W^{6+} , and most of W^{6+} was incorporated inside the SnO_2 structure at a low doping ratio from XPS study [17, 18, 21, 26]. A critical W doping level was also found as 3 at% by Kurtz et al. [56] and Zhou et al. [57] and they found that W doping improved the electrical conductivity of SnO_2 structure from theoretical calculations.

3.4 Optical properties

Optical properties of FTO and WFTO thin films have been studied by UV–VIS spectrometer at room tempe-

rate. Figure 5a shows optical transmittance curves as a function of wavelength of the thin films. From these curves, it can be seen that the transmittance of FTO film is strongly affected by the incorporation of W. It is observed that the transmittance of FTO film has an increasing tendency with W doping concentration up to 2 at% content. After this doping ratio, transmittance increases with further W doping. In addition, the absorption edge shifts towards the shorter wavelength region (blue shift) for 1 at% and 2 at% W doping and shifts to the longer wavelength region (red shift) for 3 at%, 4 at% and 5 at% W doping. The FTO and WFTO films have interference fringes, and for 3 at%, 4 at% and 5 at% W doping ratios, the interference fringes start to reduce, which implied the increase in the roughness of film surface. An increase in the roughness of the films' surface with 3 at%, 4 at% and 5 at% W doping can also be seen from AFM results. The appearance of interference fringes can indicate the smooth reflecting surface and minimum scattering loss at the surface [58].

Table 3 The electrical and optical parameter values of FTO and WFTO thin films

| Samples | R_s/Ω | Transmittance at 550 nm/% | E_g/eV | $\Phi / (10^{-2} \Omega^{-1})$ | Infrared reflectivity, $R/\%$ |
|---------|--------------|---------------------------|----------|--------------------------------|-------------------------------|
| FTO | 3.22 | 85.37 | 4.01 | 6.39 | 96.66 |
| WFTO-1 | 2.33 | 89.48 | 4.07 | 14.10 | 97.57 |
| WFTO-2 | 1.12 | 94.53 | 4.13 | 50.90 | 98.82 |
| WFTO-3 | 2.13 | 83.16 | 3.92 | 7.43 | 97.77 |
| WFTO-4 | 3.21 | 76.53 | 3.83 | 2.25 | 96.67 |
| WFTO-5 | 4.53 | 75.58 | 3.78 | 1.34 | 95.35 |

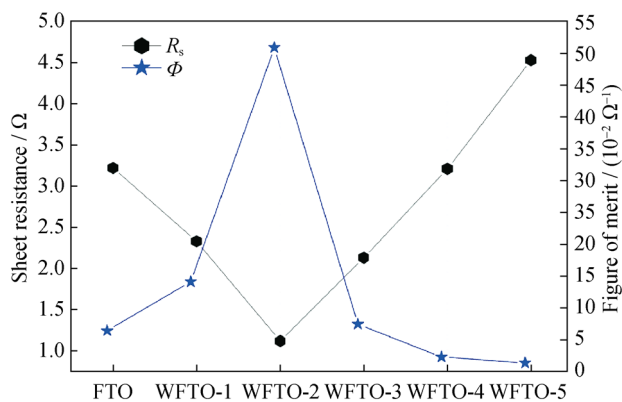


Fig. 4 W doping ratio dependence of sheet resistance and figure of merit for FTO and WFTOs thin films

The absorption coefficient (α) is determined by the following equation [30]:

$$\alpha = \ln(1/T)/d \tag{4}$$

where T is the transmittance and d is the film thickness. The optical band gap of FTO and WFTO thin films is obtained by the following relation [58]:

$$ahv = A(hv - E_g) \tag{5}$$

according to the relationship Eq. (5), where $h\nu$ and A are photon energy and the constant, respectively. E_g values are determined by plotting $(\alpha hv)^2$ versus $h\nu$ and extrapolating the linear region of the plot to zero absorption $ahv = 0$. It can be seen clearly in Fig. 5b that, when the W doping ratio is increased to 2 at% in the F-doped SnO_2 structures, the band gap value increases. After 2 at% W doping ratio, on increasing W doping ratio, band gap values sharply decrease. The band gap values of FTO, WFTO-1, -2, -3, -4 and -5 thin films are found to be 4.01, 4.07, 4.13, 3.92, 3.83 and 3.78 eV, respectively. The reason for increasing band gap with W content can probably be explained as follows: TO is a member of the degenerate semiconductor family [14], where the Fermi level is within the conduction band [53]. Thus, the optical band gap is related to the excitation

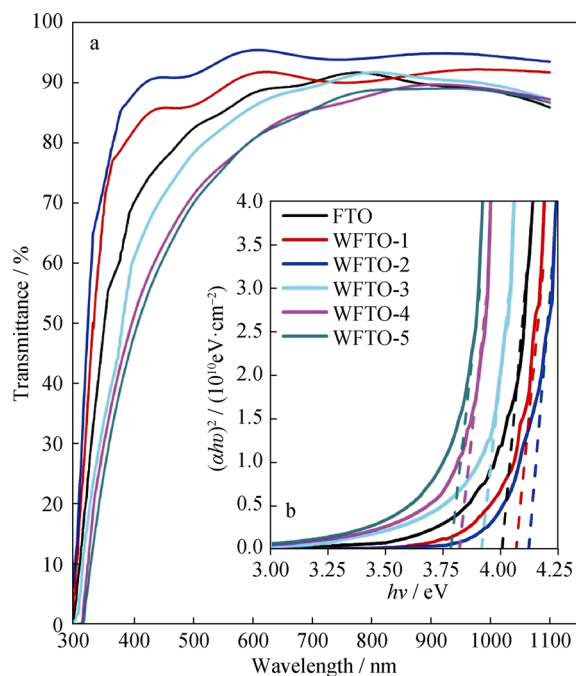


Fig. 5 a Optical transmittance and b the variation of $h\nu$ versus $(\alpha hv)^2$ for FTO and WFTOs thin films

of the electrons from the valance band to the Fermi level [36, 44]. This states that there is a rising of the Fermi level into the conduction band of the degenerate semiconductor owing to an increase in the carrier density, leading to the energy band broadening (shifting) with some of the Sn^{4+} in the lattice substituted by W^{6+} at low doping contents, which is called the Moss–Burstein effect [59]. At high doping levels, some of the W^{6+} can be reduced to the low valance states which cause a decrease in optical band gap due to energy band narrowing. Also, a decrease in E_g up to 3 at% W doping may probably be caused by the grains of layers randomly grown, which may give rise to a scattering effect. Also, reducing transmittance and band gap values can be brought about by the crystal defects, lattice strain and impurities which can be created by tungsten and fluorine doping [60]. Also, the reorientation effect observed from XRD peaks may cause a decrease in optical transmittance and optical band gap.

In solar cell applications, the figure of merit is one of significant parameters for estimating transparent conducting oxide thin films [61]. The most widely known figure of merit as described by Haacke formulation for comparing the performance of various transparent conductors is [44]

$$\Phi = T^{10}/R_s \tag{6}$$

where T is the transmittance at 550 nm and R_s is the sheet resistance. This formula makes an evaluation about whether the prepared films are appropriate as front contact for use in solar cells, and thus it is serviceably

adapted to solar cell technology. The calculated values of the figure of merit are given in Table 3 and Fig. 4. The variation of the figure of merit of FTO film with incorporation of W from Fig. 4 can be seen. When the W atoms are inserted to FTO lattice, the figure of merit increases from 6.39×10^{-2} to $50.9 \times 10^{-2} \Omega^{-1}$ up to 2 at% W doping ratio. On increasing W doping ratio further, the figure of merit values continuously decrease to the minimum value of $1.34 \times 10^{-2} \Omega^{-1}$. It is found that the WFTO-2 film has the highest value obtained in the present study. The high IR reflectivity is one of the base requirements for high quality solar windows. Further, the efficiency of flat plate collectors reduces considerably [62] due to the escape of thermal energy in the form of IR radiation. This problem is overcome by using high IR reflectivity transparent conducting oxides. The reflectivity (R) of the films can be calculated using the relation [3]

$$R = (1 + 2\varepsilon_0 c_0 R_s)^{-2} \quad (7)$$

where $\varepsilon_0 c_0 = 1/376 \Omega^{-1}$. This relation is valid over a wide range in the IR region. The estimated values of R are over 95 % and the highest value of 98.82 % is calculated for WFTO-2. Also, the IR reflectivity values are very good for IR reflective coating.

4 Conclusions

Transparent and conducting F and F + W doubly doped SnO₂ thin films have been successfully deposited on glass substrates at $(500 \pm 5)^\circ\text{C}$ by the spray pyrolysis technique. XRD study indicates that the films have polycrystalline nature with tetragonal crystal structure. It is found from XRD, SEM and AFM results that preferential orientation, grain size and grain distribution on the substrate depend on W doping content. Electrical and optical studies show that the electrical and optical properties of FTO films are changed by doping with W. In addition, the 2 at% W-doped film exhibits the lowest sheet resistance and the highest figure of merit, optical band gap and IR reflectivity. These results indicate that some properties of FTO films can be altered by W doping. Also, in comparison, the low electrical resistivity, high visible transmittance and high IR reflectivity values make 2 at% W-doped FTO film suitable for photo-thermal conversion of solar energy and transparent conductors for many optoelectronic devices applications.

References

- [1] Miao D, Zhaoa Q, Wua S, Wange Z, Zihanga X, Zhaoa X. Effect of substrate temperature on the crystal growth orientation of SnO₂:F thin films spray-deposited on glass substrates. *J Non-Cryst Solids*. 2010;356(44–49):2557.
- [2] Exarhos GJ, Zhou XD. Discovery-based design of transparent conducting oxide films. *Thin Solid Films*. 2007;515(18):7025.
- [3] Elangovan E, Ramamurthi K. Optoelectronic properties of spray deposited SnO₂:F thin films for window materials in solar cells. *J Optoelectron Adv Mater*. 2003;5(1):45.
- [4] Frank G, Kauer E, Köstlin H, Schmitte FJ. Transparent heat-reflecting coatings for solar applications based on highly doped tin oxide and indium oxide. *Sol Energy Mater*. 1983;8(4):387.
- [5] Cohen S. Low emissivity coatings for the improvement of the insulation properties of double-glazing units. *Thin Solid Films*. 1981;77(1–3):127.
- [6] Goetzberger A, Hebling C. Photovoltaic materials, past, present, future. *Sol Energy Mater Sol Cells*. 2000;62(1–2):1.
- [7] Thangaraju B. Structural and electrical studies on highly conducting spray deposited fluorine and antimony doped SnO₂ thin films from SnCl₂ precursor. *Thin Solid Films*. 2002;402(1–2):71.
- [8] Ru Q, Peng W, Zhang Z, Hu S, Li Y. First-principles calculations and experimental studies of Sn–Zn alloys as negative electrode materials for lithium-ion batteries. *Rare Met*. 2011;30(2):160.
- [9] Yi J, Li X, Hu S, Li W, Zeng R, Fu Z, Chen L. TiO₂-coated SnO₂ hollow spheres as anode materials for lithium ion batteries. *Rare Met*. 2011;30(6):589.
- [10] Elangovan E, Shivashankar SA, Ramamurthi K. Studies on structural and electrical properties of sprayed SnO₂:Sb films. *J Cryst Growth*. 2005;276(1–2):215.
- [11] Elangovan E, Singh MP, Ramamurthi K. Studies on structural and electrical properties of spray deposited SnO₂:F thin films as a function of film thickness. *Mater Sci Eng B*. 2004;113(2):143.
- [12] Chung WY, Shim CH, Choi SD, Lee DD. Tin oxide microsensor for LPG monitoring. *Sens Actuators B*. 1994;20(2–3):139.
- [13] Moholkar AV, Pawar SM, Rajpure KY, Patil PS, Bhosale CH. Properties of highly oriented spray-deposited fluorine-doped tin oxide thin films on glass substrates of different thickness. *J Phys Chem Solids*. 2007;68(10):1981.
- [14] Batzill M, Diebold U. The surface and materials science of tin oxide (review). *Prog Surf Sci*. 2005;79(2–4):47.
- [15] Kılıç C, Zunger A. Origins of coexistence of conductivity and transparency in SnO₂. *Phys Rev Lett*. 2002;88(9):095501.
- [16] Nunes P, Fortunato E, Tonello P, Fernandes FB, Vilarinho P, Martins R. Effect of different dopant elements on the properties of ZnO thin films. *Vacuum*. 2002;64(3–4):281.
- [17] Huang Y, Li G, Feng J, Zhang Q. Investigation on structural, electrical and optical properties of tungsten-doped tin oxide thin films. *Thin Solid Films*. 2010;518(8):1892.
- [18] Huang Y, Li D, Feng J, Li G, Zhang Q. Transparent conductive tungsten-doped tin oxide thin films synthesized by sol-gel technique on quartz glass substrates. *J Sol-Gel Sci Technol*. 2010;54(3):276.
- [19] Moholkar AV, Pawar SM, Rajpure KY, Bhosale CH, Kim JH. Effect of fluorine doping on highly transparent conductive spray deposited nanocrystalline tin oxide thin films. *Appl Surf Sci*. 2009;255(23):9358.
- [20] Ramaiah KS, Raja VS. Structural and electrical properties of fluorine doped tin oxide films prepared by spray-pyrolysis technique. *Appl Surf Sci*. 2006;253(3):1451.
- [21] Huang Y, Zhan Q, Li G. Transparent conductive tungsten-doped tin oxide polycrystalline films prepared on quartz substrates. *Semicond Sci Technol*. 2009;24(1):015003.
- [22] Moholkar AV, Pawar SM, Rajpure KY, Almari SN, Patil PS, Bhosale CH. Solvent-dependent growth of sprayed FTO thin films with mat-like morphology. *Sol Energy Mater Sol Cells*. 2008;92(11):1439.

- [23] Qignan Z, Sjuo W, Dengkui M. Effect of substrate temperature on the haze and properties of SnO₂:F thin film coated on glass (FTO) by spray pyrolysis process. *Adv Mater Res.* 2011; 150–151:1043.
- [24] Shewale PS, Patil SI, Uplane MD. Preparation of fluorine-doped tin oxide films at low substrate temperature by an advanced spray pyrolysis technique, and their characterization. *Semicond Sci Technol.* 2010;25(3):15008.
- [25] Chen Q, Qian Y, Chen Z, Zhou G, Zhang Y. Fabrication of ultrafine SnO₂ thin films by the hydrothermal method. *Thin Solid Films.* 1995;264(1):25.
- [26] Huang Y, Zhang Q, Li G, Yang M. Tungsten-doped tin oxide thin films prepared by pulsed plasma deposition. *Mater Charact.* 2009;60(5):415.
- [27] Nakao S, Yamada N, Hitosugi T, Hirose Y, Shimada T, Hasegawa T. Fabrication of transparent conductive W-doped SnO₂ thin films on glass substrates using anatase TiO₂ seed layers. *Phys Status Solidi C.* 2011;8(2):543.
- [28] Muranaka S, Band Y. Reactive deposition of W-, Mo- and V-doped SnO films. *Bull Inst Chem Res Kyoto Univ.* 1992;70:430.
- [29] Elangovan E, Singh MP, Dharmaprakash MS, Ramamurthi K. Some physical properties of spray deposited SnO₂ thin films. *J Optoelectron Adv Mater.* 2004;6(1):197.
- [30] Serin T, Serin N, Karadeniz S, Sari H, Tugluoglu N, Pakma O. Electrical, structural and optical properties of SnO₂ thin films prepared by spray pyrolysis. *J Non-Cryst Solids.* 2006;352(3):209.
- [31] Gordillo G, Moreno LC, de la Cruz W, Teheran P. Preparation and characterization of SnO₂ thin films deposited by spray pyrolysis from SnCl₂ and SnCl₄ precursors. *Thin Solid Films.* 1994;252(1):61.
- [32] Smith A, Laurent JM, Smith DS, Bonnet JP, Clemente RR. Relation between solution chemistry and morphology of SnO₂-based thin films deposited by a pyrosol process. *Thin Solid Films.* 1995;266(1):20.
- [33] Agashe C, Takwale MG, Bhide VG, Mahamuni S, Kulkarni SK. Effect of Sn incorporation on the growth mechanism of sprayed SnO₂ films. *J Appl Phys.* 1991;70(12):7382.
- [34] Elangovan E, Ramamurthi K. Studies on micro-structural and electrical properties of spray-deposited fluorine-doped tin oxide thin films from low-cost precursor. *Thin Solid Films.* 2005; 476(2):231.
- [35] Elangovan E, Ramamurthi K. A study on low cost-high conducting fluorine and antimony-doped tin oxide thin films. *Appl Surf Sci.* 2005;249(1–4):183.
- [36] Babar AR, Shinde SS, Moholkar AV, Bhosale CH, Kim JH, Rajpure KY. Sensing properties of sprayed antimony doped tin oxide thin films; solution molarity. *J Alloy Compd.* 2011;509(6):3108.
- [37] Chacko S, Philip NS, Gopchandran KG, Koshy P, Vaidyan VK. Nanostructural and surface morphological evolution of chemically sprayed SnO₂ thin films. *Appl Surf Sci.* 2008;254(7):2179.
- [38] Lin CC, Chiang MC, Chen YW. Temperature dependence of fluorine-doped tin oxide films produced by ultrasonic spray pyrolysis. *Thin Solid Films.* 2009;518(4):1241.
- [39] Agashe C, Hüpkens J, Schöpe G, Berginski M. Physical properties of highly oriented spray-deposited fluorine-doped tin dioxide films as transparent conductor. *Sol Energy Mater Sol Cells.* 2009;93(8):1256.
- [40] Agashe C, Major SS. Effect of Heavy doping in SnO₂:F films. *J Mater Sci.* 1996;31(11):2965.
- [41] Patil PS, Kawar RK, Seth T, Amalnerkar DP, Chigare PS. Effect of substrate temperature on structural, electrical and optical properties of sprayed tin oxide (SnO₂) thin films. *Ceram Int.* 2003;29(7):725.
- [42] Zaouk D, Asmar R, Podlecki J, Zaatar Y, Khoury A, Foucaran A. X-ray diffraction studies of electrostatic sprayed SnO₂:F films. *Microelectron J.* 2007;38(8–9):884.
- [43] Shanthi S, Subramanian C, Ramasamy P. Preparation and properties of sprayed undoped and fluorine doped tin oxide films. *Mater Sci Eng B.* 1999;57(2):127.
- [44] Babar AR, Shinde SS, Moholkar AV, Bhosale CH, Kim JH, Rajpure KY. Structural and optoelectronic properties of antimony incorporated tin oxide thin films. *J Alloy Compd.* 2010; 505(2):416.
- [45] Yao P. Effects of Sb doping level on the properties of Ti/SnO₂–Sb electrodes prepared using ultrasonic spray pyrolysis. *Desalination.* 2011;267(2–3):170.
- [46] Kasar RR, Deshpande NG, Gudage YG, Vyas JC, Sharma R. Studies and correlation among the structural, optical and electrical parameters of spray-deposited tin oxide (SnO₂) thin films with different substrate temperatures. *Physica B.* 2008; 403(19–20):3724.
- [47] Jadsadapattarakul D, Euvananont C, Thanachayanont C, Nukeaw J, Sooknoi T. Tin oxide thin films deposited by ultrasonic spray pyrolysis. *Ceram Int.* 2008;34(4):1051.
- [48] Bedir M, Öztaş M, Bakkaoglu OF, Ormanel R. Investigations on structural, optical and electrical parameters of spray deposited ZnSe thin films with different substrate temperature. *Eur Phys J B.* 2005;45(4):465.
- [49] Dhanam M, Manoj PK, Rajeev R, Prabhu R. High-temperature conductivity in chemical bath deposited copper selenide thin films. *J Cryst Growth.* 2005;280(3–4):425.
- [50] Moholkar AV, Pawar SM, Rajpure KY, Bhosale CH. Effect of concentration of SnCl₄ on sprayed fluorine doped tin oxide thin films. *J Alloy Compd.* 2008;455(1–2):440.
- [51] Yadav AA, Masumdar EU, Moholkar AV, Neumann-Spallart M, Rajpure KY, Bhosale CH. Electrical, structural and optical properties of SnO₂:F thin films: effect of the substrate temperature. *J Alloy Compd.* 2009;488(1):350.
- [52] Ouerfelli J, Djobo SO, Bernède JC, Cattin L, Morsli M, Berredjem Y. Organic light emitting diodes using fluorine doped tin oxide thin films, deposited by chemical spray pyrolysis, as anode. *Mater Chem Phys.* 2008;112(1):198.
- [53] Lingane JJ, Small LA. Polarography of the various oxidation states of tungsten. *J Am Chem Soc.* 1949;71(3):973.
- [54] Lassner E, Schubert W-D. Tungsten. New York: Kluwer Academic; 1999.
- [55] Greenwood NN, Earnsha A. Chemistry of the Elements. 2nd ed. Oxford: Elsevier; 1997.
- [56] Kurtz A, Brakecha K, Puetz J, Aegerter MA. Strategies for novel transparent conducting sol–gel oxide coatings. *Thin Solid Films.* 2006;502(1–2):212.
- [57] Zhou W, Liu L, Yuan M, Song Q, Wu P. Electronic and optical properties of W-doped SnO₂ from first-principles calculations. *Comput Mater Sci.* 2012;54:109.
- [58] Keskenler EF, Turgut G, Doğan S. Investigation of structural and optical properties of ZnO films co-doped with fluorine and indium. *Superlattices Microstruct.* 2012;52(1):107.
- [59] Burstein E. Anomalous optical absorption limit in InSb. *Phys Rev.* 1954;93(3):632.
- [60] Yakuphanoglu F, Caglar Y, Ilican S, Caglar M. The effects of fluorine on the structural, surface morphology and optical properties of ZnO thin films. *Physica B.* 2007;394(1):86.
- [61] Memarian N, Rozati SM, Elemurugu E, Fortunato E. Characterization of SnO₂:F thin films deposited by an economic spray pyrolysis technique. *Phys Status Solidi C.* 2010;7(9):2277.
- [62] Frank G, Kauer E, Kostlin H. Transparent heat-reflecting coatings based on highly doped semiconductors. *Thin Solid Films.* 1981;77(1–3):107.